Supporting Information

Overall water splitting reaction catalyzed by a novel bi-functional Ru/Ni_3N-Ni electrode

Zong Liu[a,b], Meng Zha[a,b], Quan Wang[a], Guangzhi Hu[b] and Ligang Feng[*b]*

a Key Laboratory of Medicinal Chemistry for Natural Resource (Yunnan University), Ministry of Education, School of Chemical Science and Engineering, Yunnan University, Kunming 650091, Yunnan, China

b School of Chemistry and Chemical Engineering, Yangzhou University, Yangzhou 225002, China

[*]Corresponding authors

E-mail addresses: ligang.feng@yzu.edu.cn, fenglg11@gmail.com (L. Feng*). ORCID: 0000-0001-9879-0773 ; guangzhihu@ynu.edu.cn (G. Hu)

Experimental Section

Synthesis of Ni_3N-Ni. 1 mmol of Ni $(NO_3)_2 \cdot 6H_2O$ and 1 mmol KOH was dissolved in a 30 mL deionized water under vigorous stirring for 30 min; then, the precipitate was obtained by a filter and cleaned with deionized water and ethanol several times, respectively. The obtained precipitate by drying at 60 °C for 8 h under a vacuum atmosphere. The Ni_3N-Ni was synthesized by the nitriding of precipitate under NH_3 atmosphere at 420 °C for 3h in a tube furnace. The obtained powder sample was washed by water and ethanol and then dried at 60 °C for 12 h under vacuum.

Synthesis of Ru/Ni_3N-Ni. The obtain Ni_3N-Ni sample and $RuCl_3$ was dispersed in the ethanol under stirring. Then the mixture was dried at 60 °C for 8 h under a vacuum atmosphere. The mass ratio of Ni_3N-Ni and $RuCl_3$ was 1:1. The mixture was thermally reduced under the H_2 atmosphere at 300 °C for 2h to obtain the Ru/Ni_3N-Ni sample. The powder was washed by water and ethanol, and then dried at 60 °C for 12 h under vacuum.

Synthesis of Ru. The $RuCl_3$ powder was drying at 60 °C for 8 h under a vacuum atmosphere. The powder was thermally reduced under the H_2 atmosphere at 300 °C for 2h to obtain the Ru sample. The powder was washed by water and ethanol, and then dried at 60 °C for 12 h under vacuum.

Characterization

Powder X-ray diffraction (XRD) patterns were recorded on a Bruker D8 Advance Powder X-ray diffractometer using a Cu Kα (λ = 1.5405 Å) radiation source operating at 40 kV and 40 mA, and at a scanning rate of 5 ° min^{-1}. A fine powder sample was ground, then put on the glass slide and pressed to make a flat surface under the glass slide. All transmission electron microscopy (TEM) and high-resolution TEM (HRTEM) measurements were conducted on a TECNAI G2 operating at 200 kV. The element mapping analysis and energy-dispersive X-ray detector spectrum (EDX) images were obtained on a TECNAI G2 transmission electron microscope equipped with an EDXA detector: the microscope was operated at an acceleration voltage of 200

kV. All X-Ray photoelectron spectroscopy (XPS) measurements were carried out on a Kratos XSAM-800 spectrometer with an Al Kα radiation source.

All the electrochemical measurements were performed with a Bio-Logic VSP electrochemical workstation (Bio-Logic Co., France). The OER and HER performance were measured in a three-electrode electrochemical cell. A saturated calomel electrode (SCE, Hg/Hg_2Cl_2) electrode was used as the reference electrode through a double salt-bridge and luggin capillary tip, and it was carefully calibrated before and after the measurement to ensure the accuracy. A graphite rod was used as the counter electrode. Potentials were referenced to a reversible hydrogen electrode (RHE) by adding a value of (0.24 + 0.0592*pH) V. A glassy carbon electrode (3.0 mm in diameter) was used as the working electrode. The glassy carbon electrode was polished separately by 1 micron and 50-nanometer alumina powder. And then the electrode was cleaning in ultrapure water several times and dried at room temperature before use. The current density was normalized over the geometric surface area of the electrode (0.07 cm^2). All potentials were converted and referred to the RHE unless stated otherwise.

A total electrolyte volume of ~50 mL was used to fill the glass cell. The cyclic voltammetry experiments for the OER and HER were conducted in 1 M KOH at 25 °C using a working electrode and a scan rate of 5 mV s^{-1}. The preparation of the samples was shown in detail as follows: 2 mg of Ru/Ni_3N-Ni or Ni_3N-Ni or Ru, 1 mg of Pt/C or RuO_2 catalysts, 960 μL ethanol and 40 μL Nafion solution were mixed, and then sonicated for 30 min to make a homogeneous dispersion. 6 μL of the catalysts ink was loaded onto the glassy carbon electrode by drop-casting as the working electrode. Prior to recording the OER and HER activity of as-preparation catalysts, the catalysts were activated by 50 cyclic voltammetry scans in 1 M KOH at a scan rate of 50 mV s^{-1}. The liner scan voltammogram (LSV) curves were obtained by sweeping the potential from 1.2 to 1.8 V for OER and 0 to -0.4 V for HER at room temperature, with a sweep rate of 5 mV s^{-1}. Tafel plots were recorded at a scan rate of 5 mV s^{-1} via CV curves. Electrochemical impedance spectroscopy (EIS) determination was conducted in the frequency range from 1000 kHz to 0.01Hz. The durability test was carried out for 1000 cycles within the potential ranging from 1.2 to 1.8 V for OER and 0 to -0.4 V for HER in 1 M KOH at a scan rate of 50 mV s^{-1}, and a linear sweep was measured under a sweep rate of 5 mV s^{-1} after 1000 cycles. Chronoamperometry (CA) was carried out to estimate the stability of the catalyst at the potential of 1.43 V vs. RHE for OER and -53

mV vs. RHE for HER for 20 hours.

The electrochemical surface area (ECSA) was evaluated in terms of doubler layer capacitance (C_{dl}). The ECSA was estimated by cyclic voltammetry (CV) without Faradaic processes occurred region from 0.925 to 1.125 V in 1 M KOH at scan rate 20, 40, 60, 80 and 100 mV s^{-1}. The C_{dl} was estimated by plotting the $\Delta J = (J_a - J_c)/2$ at 1.025 V vs. RHE against the scan rate. The linear slope is the double layer capacitance $C_{dl.}$ The specific capacitance is evaluated for a flat surface by assuming 40 μF cm^{-2} according to previous literature.[1] The electrochemically active surface area was achieved by normalizing the doubler layer capacitance to a standard specific capacitance.

Turnover frequency (TOF) was calculated using the following equation (lower TOF limits were calculated) [2]:

$$OER: TOF = \frac{J \times A}{(4 \times F \times n)}$$

$$HER: TOF = \frac{J \times A}{(2 \times F \times n)}$$

J is the current density at a specific overpotential (A cm^{-2}). *A* is the geometric area of the work electrode samples. *F* is the Faraday constant (96485 mol C^{-1}). *n* is the total number of moles of all the active metal sites (Ru and Ni metal ions) that were deposited onto the glassy carbon electrode.

A gas-tight electrochemical cell coupling with a gas burette was carried out to verify the faradaic yield of samples. The working electrode was prepared by drop-casting catalyst suspension on the glassy carbon electrode with the surface area of 0.07 cm^{-2}. A constant overpotential (53 mV and 1.43 V) was applied on the electrode and the volume of the evolved gas was recorded synchronously. Thus, the faradaic yield was calculated from the ratio of the recorded gas volume to the theoretical gas volume during the charge passed through the electrode[3]:

$$Faradaic\ yield = \frac{V_{experimental}}{V_{theoretical}} = \frac{V_{experimental}}{\frac{1(2)}{4} \times \frac{Q}{F} \times V_m}$$

where *Q* is the charge passed through the electrode, *F* is Faraday constant (96485 C mol^{-1}), the number 4 means 4 mole electrons per mole O_2, the number 1 (2) means 1 O_2 (2 mole H_2) mole, V_m is molar volume of gas (24.5 L mol^{-1}, 298 K, 101 KPa).

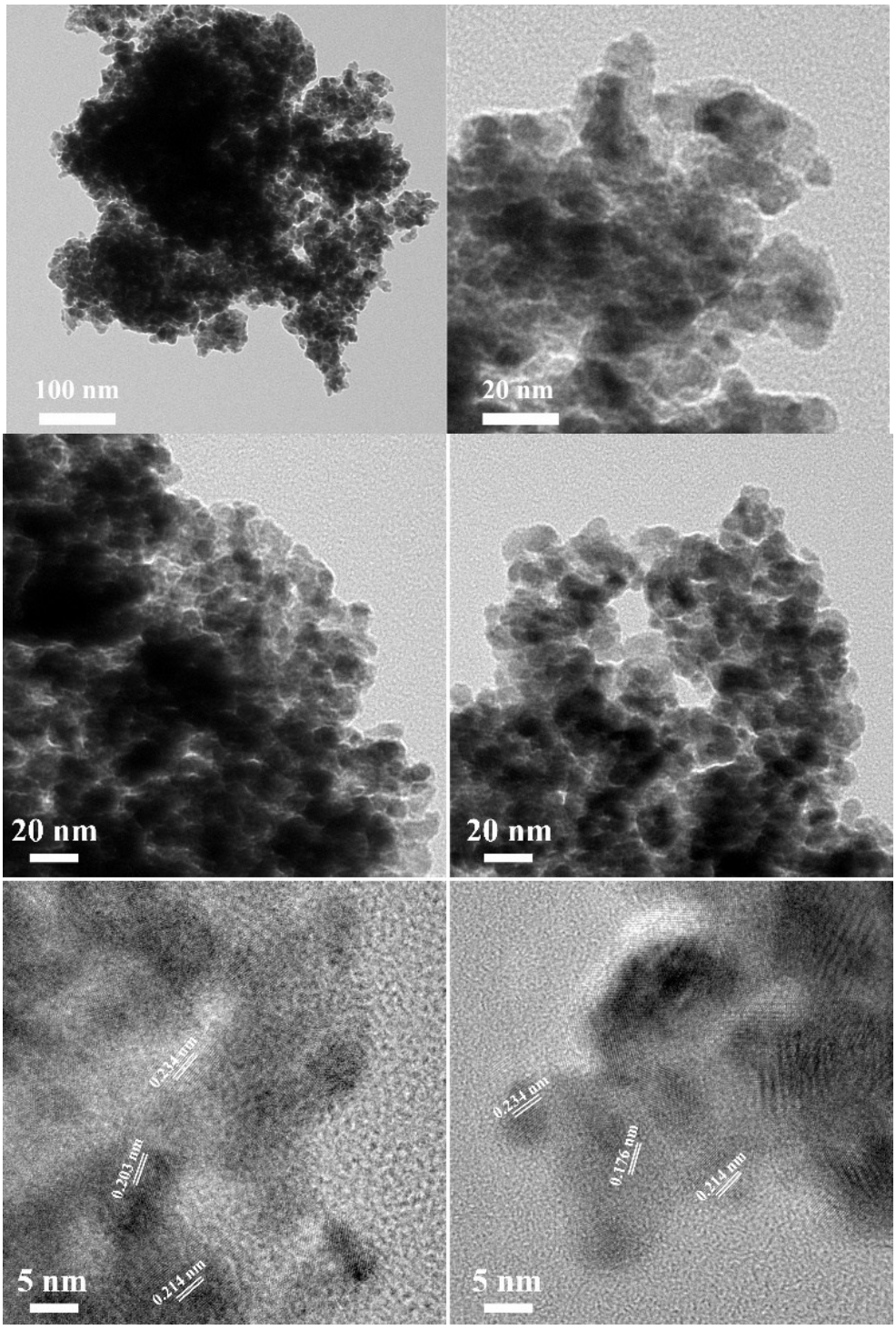

Figure S1. Additional TEM and HRTEM images of the Ru/Ni_3N-Ni.

The high-resolution TEM (HRTEM) images showed the lattice spacing of about 0.234 nm attributed to the (100) plane of Ru ; Other lattice spacing of about 0.203 nm for the (111) plane of metal Ni or Ni_3N, 0.214 nm for the (002) plane of metal Ru or Ni_3N, and 0.176 nm for the (200) plane of metal Ni.

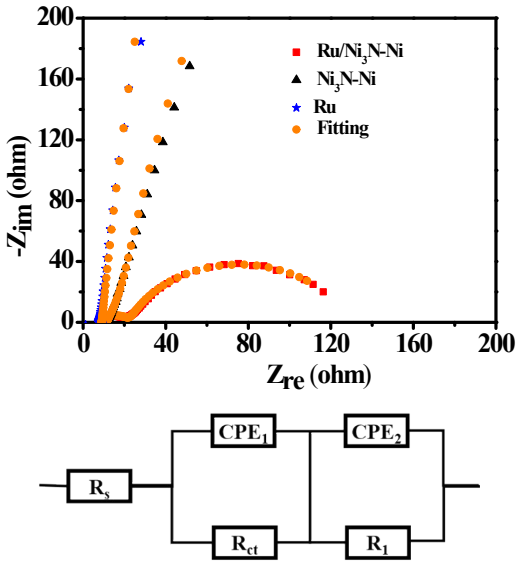

Figure S2. Nyquist plots and the equivalent circuit model of Ru/Ni_3N-Ni, Ni_3N-Ni and Ru.

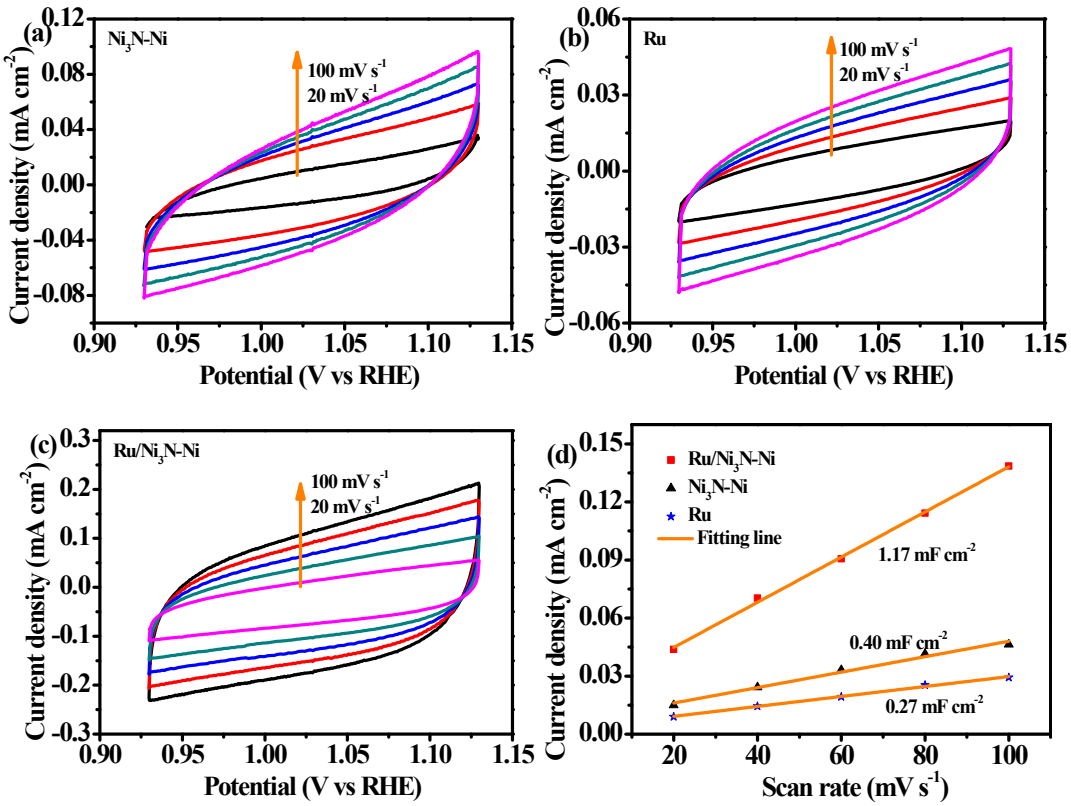

Figure S3. Cyclic voltammograms of (a) Ni_3N-Ni, (b) Ru, and (c) Ru/Ni_3N-Ni in the non-faradaic capacitance current range from 0.925 V to 1.125 V vs. RHE at scan rates of 20, 40, 60, 80 and 100 mV/s, (d) Current density as a function of the scan rate for the different electrodes.

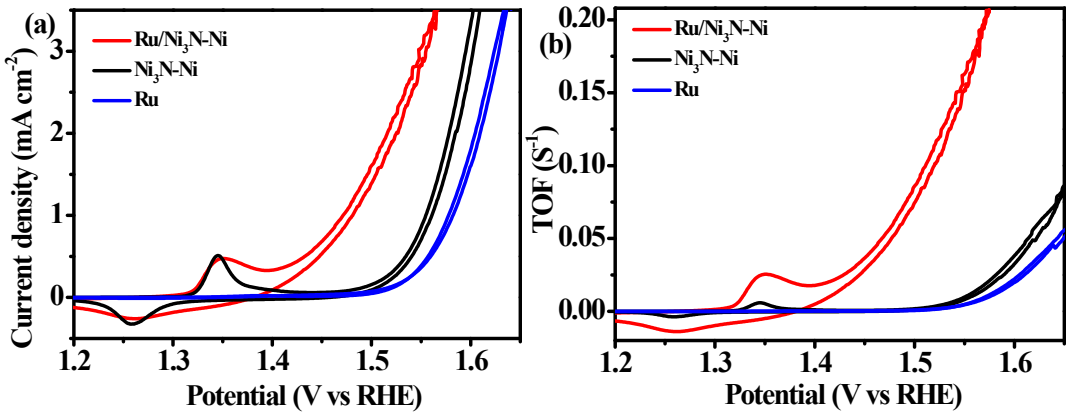

Figure S4. (a) The specific activity of Ru/Ni_3N-Ni, Ni_3N-Ni and Ru by normalizing the raw current to the electrochemical surface area, (b) TOF value of the Ru/Ni_3N-Ni, Ni_3N-Ni and Ru as a function of potentials.

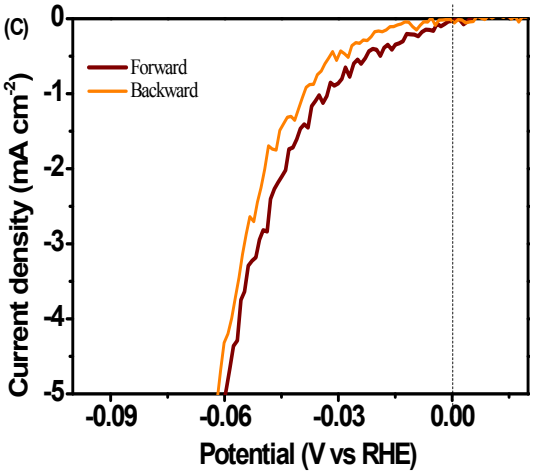

Figure S4. (c) Forward and backward scanning polarization curves of Pt/C in the range from 0 to 5 mA cm^{-2}. The thermodynamic potential of 0 V was indicated by dash line.

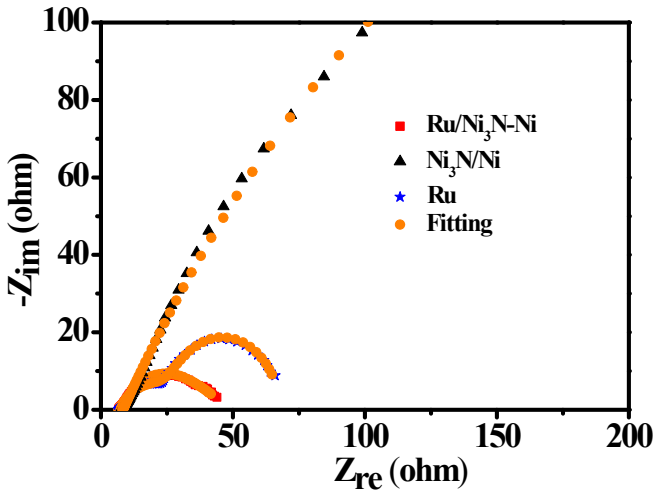

Figure S5. Nyquist plots of Ru/Ni_3N-Ni, Ni_3N-Ni and Ru.

By fitting the Nyquist plot using an equivalent circuit, the smallest charge transfer resistance of Ru/Ni_3N-Ni catalyst, less than that of Ni_3N-Ni and Ru indicating more rapid kinetics.

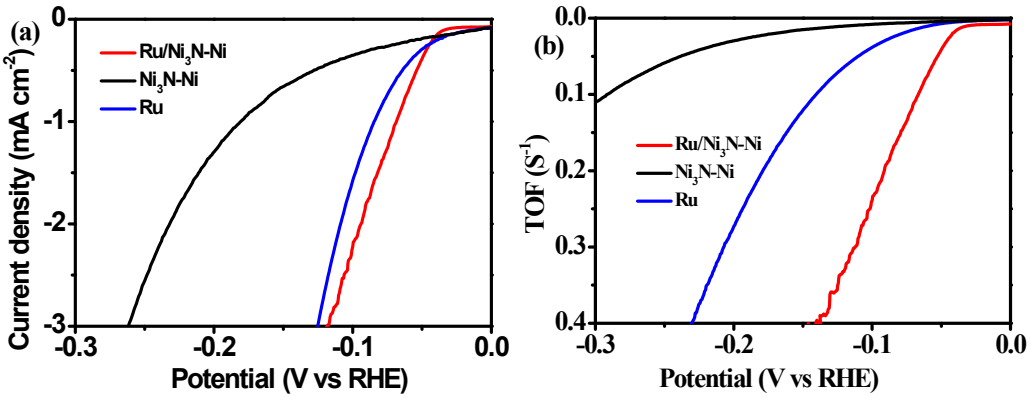

Figure S6. (a) Specific HER activity of as-prepared catalysts. Polarization curves are normalized by the electrochemical active surface areas, which indicates the higher specific activity of the Ru/Ni_3N-Ni, Ni_3N-Ni and Ru. (b) TOF values of the Ru/Ni_3N-Ni, Ni_3N-Ni and Ru as a function of overpotential.

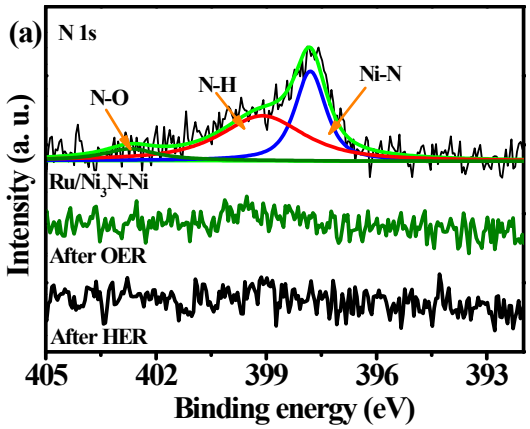

Figure S7. XPS spectra of the N 1s regions of Ru/Ni_3N-Ni and after OER and HER characterization.

Table S1. The surface composition of Ni_3N-Ni, Ru and Ru/Ni_3N-Ni derived from XPS and EDX spectrum.

Samples	C 1s at%	O 1s at%	N 1s at%	Ni 2p at%	Ru 2p at%
Ru/Ni_3N-Ni[a]	28.4	48.6	2.9	13.0	7.1
Ni_3N-Ni	25.1	44.4	8.7	25.1	-
Ru	53.1	27.1	-	-	19.8
Ru/Ni_3N-Ni[b]	38.5	7.1	2.7	22.3	29.4

a): XPS spectrum, b) EDX spectrum

Table S2. The comparison of some representative OER electrocatalysts in alkaline electrolytes.

Materials	Electrolyte (KOH)	Electrode substrate	Overpotential η_{10} (mV)	Reference
Ru/Ni_3N-Ni	1 M KOH	GCE[a]	200	This work
RuO_2	1 M KOH	GCE	315	This work
$Ni_{1.25}Ru_{0.75}P$	1 M KOH	GCE	340	[4]
RuS_2-500	1 M KOH	GCE	282	[5]
Ru-RuP_x-Co_xP	0.1 M KOH	GCE	291	[6]
RuO_2	1 M KOH	GCE	370	[7]
RuO_2/Co_3O_4	1 M KOH	GCE	305	[8]
$CoSe_{2-x}$-Pt	1 M KOH	GCE	255	[9]
Rh-V_{CC}	1 M KOH	GCE	350	[10]
Co@Ir/NC-10%	1 M KOH	GCE	280	[11]
IrO_2	1 M KOH	GCE	360	[12]
Pt-CoS_2/CC	1 M KOH	CC	300	[13]
Ru_2Ni_2 SNs/C	1 M KOH	GCE	310	[14]

a) GCE: glassy carbon electrode;

Table S3. EIS fitting parameters from equivalent circuit of Ru/Ni_3N-Ni at different overpotential for OER.

Ru/Ni_3N-Ni	R_s / Ω cm^{-2}	R_1 / Ω cm^{-2}	CPE_1 / S s^{-n}	n / 0<n<1	R_{ct} / Ω cm^{-2}	CPE / S s^{-n}	n / 0<n<1
160 mV	8.0	12.7	5.43E-4	0.69	565	2.08E-2	0.84
180 mV	8.0	14.8	5.31E-4	0.65	238	2.02E-2	0.83
200 mV	7.6	14.4	5.22E-3	0.50	103	1.96E-2	0.79
220 mV	7.9	13.9	4.68E-3	0.47	53.0	1.91E-2	0.69
240 mV	7.8	12.0	3.79E-3	0.46	25.1	1.81E-2	0.65

Table S4. EIS fitting parameters from equivalent circuit of samples at 200 mV overpotential.

Samples	R_s / Ω cm^{-2}	R_1 / Ω cm^{-2}	CPE_1 / S s^{-n}	n / 0<n<1	R_{ct} / Ω cm^{-2}	CPE / S s^{-n}	n / 0<n<1
Ru/Ni_3N-Ni	7.6	14.4	5.22E-3	0.50	103	1.96E-2	0.79
Ni_3N-Ni	8.0	29.6	1.36E-1	0.62	2109	2.47E-3	0.97
Ru	7.7	3280	1.45E-5	0.96	20130	1.39E-5	0.94

Table S5. The comparison of some representative Ru based HER electrocatalysts with our work in alkaline electrolytes.

Materials	Electrolyte (KOH)	Electrode substrate	Overpotential η_{10} (mV)	Reference
Ru/Ni_3N-Ni	1 M KOH	GCE[a]	53	This work
Pt/C	1 M KOH	GCE	60	This work
RuP_2 nanoparticles	1 M KOH	GCE	90	[15]
1D-RuO_2-CN_x	0.5 M KOH	g-Carbon Nitride	95	[16]
Pt@C_2N	1 M KOH	GCRDE[b]	100	[17]
Ru/C_3N_4/C	0.1 M KOH	GCRDE	79	[18]
Ru/C	0.1 M KOH	GCRDE	120	[18]
Pt/C	0.1 M KOH	GCRDE	90	[18]
$Co(OH)_2$/Pt(111)	0.1MKOH	GCRDE	248	[19]
$NiCo_2S_4$/Pd	1 M KOH	GCE	87	[20]
RuS_2-500	1 M KOH	GCE	79	[5]
RuP/NPC	1 M KOH	Ni foam	168	[21]
RuO_2/Co_3O_4	1 M KOH	GCE	89	[8]
Co@Ir/NC-10%	1 M KOH	GCE	121	[11]
$Cu_{2-x}S$@Ru	1 M KOH	GCRDE	82	[22]

a) GCE: glassy carbon electrode; b) GCRDE: glass carbon rotating disk electrode

Table S6. EIS fitting parameters from equivalent circuit of Ru/Ni_3N-Ni at different overpotential for HER.

Ru/Ni_3N-Ni	R_s / Ω cm^{-2}	R_1 / Ω cm^{-2}	CPE_1 / S s^{-n}	n / 0<n<1	R_{ct} / Ω cm^{-2}	CPE / S s^{-n}	n / 0<n<1
20 mV	7.9	19.1	5.25E-3	0.81	650	6.21E-2	0.98
40 mV	7.5	18.5	5.05E-3	0.78	120	6.16E-2	0.87
60 mV	7.6	17.5	4.58E-3	0.74	30.1	3.66E-2	0.43
80 mV	7.8	16.8	4.08E-3	0.73	8.8	2.76E-2	0.38
100 mV	7.6	16.0	3.78E-3	0.72	2.4	1.93E-2	0.36

Table S7. EIS fitting parameters from equivalent circuit of Ru/Ni_3N-Ni at 60 mV overpotential.

Samples	R_s / Ω cm^{-2}	R_1 / Ω cm^{-2}	CPE_1 / S s^{-n}	n / 0<n<1	R_{ct} / Ω cm^{-2}	CPE / S s^{-n}	n / 0<n<1
Ru/Ni_3N-Ni	7.6	17.5	4.58E-3	0.74	30.1	3.66E-2	0.43
Ni_3N-Ni	7.8	252.3	2.61E-2	0.5	510	3.54E-3	0.66
Ru	7.5	19.4	5.31E-3	0.65	41.9	3.98E-2	0.89

Table S8. Summary of some reported representative noble metal-based water splitting electrocatalysts

Materials	Electrolyte (KOH)	Electrode substrate	Overall potential V at 10 mA cm^{-2}	Reference
Ru/Ni_3N-Ni||Ru/Ni_3N-Ni	1 M KOH	GCE[a]	1.49	This work
RuO_2||Pt/C	1 M KOH	GCE	1.61	This work
Pt/C||Ir/C	1 M KOH	Ni foam	1.6	[23]
Pt/C||Ir/C	1 M KOH	GCE	1.56	[24]
Co@Ir/NC-10%||Co@Ir/NC-10%	1 M KOH	GCE	1.667	[11]
RuO_2/Co_3O_4||RuO_2/Co_3O_4	1 M KOH	GCE	1.645	[8]
Rh_xP/NPC||Rh_xP/NPC	1 M KOH	GCE	1.64	[21]
Ir_1@Co/NC||Ir_1@Co/NC	1 M KOH	GCE	1.6	[25]
Pt-CoS_2/CC||Pt-CoS_2/CC	1 M KOH	CC	1.55	[13]
Ru_2Ni_2 SNs/C||Ru_2Ni_2 SNs/C	1 M KOH	CFP	1.58	[14]

a) glass carbon electrode; b) glass carbon rotating disk electrode

References

[1] a) C. C. L. McCrory, S. Jung, I. M. Ferrer, S. M. Chatman, J. C. Peters, T. F. Jaramillo, *J. Am. Chem. Soc.* **2015**, *137*, 4347-4357; b) C. C. L. McCrory, S. Jung, J. C. Peters, T. F. Jaramillo, *J. Am. Chem. Soc.* **2013**, *135*, 16977-16987; c) Y. Ruquan, d. A. V. Paz, L. Yuanyue, A. J. M. Josefina, P. Zhiwei, W. Tuo, L. Yilun, Y. B. I., W. Su-Huai, Y. M. Jose, T. J. M., *Adv. Mater.* **2016**, *28*, 1427-1432; d) G. Dingyi, Q. Jing, Z. Wei, C. Rui, *ChemSusChem* **2017**, *10*, 394-400.

[2] a) L. Trotochaud, J. K. Ranney, K. N. Williams, S. W. Boettcher, *J. Am. Chem. Soc.* **2012**, *134*, 17253-17261; b) J. Jiang, A. Zhang, L. Li, L. Ai, *J. Power Sources* **2015**, *278*, 445-451.

[3] W. Jun, L. Kai, Z. Hai-xia, X. Dan, W. Zhong-li, J. Zheng, W. Zhi-jian, Z. Xin-bo, *Angew. Chem., Int. Ed.* **2015**, *54*, 10530-10534.

[4] D. R. Liyanage, D. Li, Q. B. Cheek, H. Baydoun, S. L. Brock, *J. Mater. Chem. A* **2017**, *5*, 17609-17618.

[5] Y. Zhu, H. A. Tahini, Y. Wang, Q. Lin, Y. Liang, C. M. Doherty, Y. Liu, X. Li, J. Lu, S. C. Smith, C. Selomulya, X. Zhang, Z. Shao, H. Wang, *J. Mater. Chem. A* **2019**, *7*, 14222-14232.

[6] L. Wang, Q. Zhou, Z. Pu, Q. Zhang, X. Mu, H. Jing, S. Liu, C. Chen, S. Mu, *Nano Energy* **2018**, *53*, 270-276.

[7] D. Li, H. Baydoun, B. Kulikowski, S. L. Brock, *Chem. Mater.* **2017**, *29*, 3048-3054.

[8] H. Liu, G. Xia, R. Zhang, P. Jiang, J. Chen, Q. Chen, *RSC Adv.* **2017**, *7*, 3686-3694.

[9] L. Zhuang, Y. Jia, H. Liu, X. Wang, R. K. Hocking, H. Liu, J. Chen, L. Ge, L. Zhang, M. Li, C.-L. Dong, Y.-C. Huang, S. Shen, D. Yang, Z. Zhu, X. Yao, *Adv. Mater.* **2019**, *31*, 1805581.

[10] Y. Zhou, G. Gao, J. Kang, W. Chu, L.-W. Wang, *J. Mater. Chem. A* **2019**, *7*, 12050-12059.

[11] D. Li, Z. Zong, Z. Tang, Z. Liu, S. Chen, Y. Tian, X. Wang, *ACS Sustainable Chem. Eng.* **2018**, *6*, 5105-5114.

[12] A. Dutta, A. K. Samantara, S. K. Dutta, B. K. Jena, N. Pradhan, *ACS Energy Lett.* **2016**, *1*, 169-174.

[13] X. Han, X. Wu, Y. Deng, J. Liu, J. Lu, C. Zhong, W. Hu, *Adv. Energy Mater.* **2018**, *8*, 1800935.

[14] J. Ding, Q. Shao, Y. Feng, X. Huang, *Nano Energy* **2018**, *47*, 1-7.

[15] Z. Pu, I. S. Amiinu, Z. Kou, W. Li, S. Mu, *Angew. Chem., Int. Ed.* **2017**, *56*, 11559-11564.

[16] T. Bhowmik, M. K. Kundu, S. Barman, *ACS Appl. Mater. Interfaces* **2016**, *8*, 28678-28688.

[17] J. Mahmood, F. Li, S. M. Jung, M. S. Okyay, I. Ahmad, S. J. Kim, N. Park, H. Y. Jeong, J. B. Baek, *Nat. Nanotechnol.* **2017**, *12*, 441-446.

[18] Y. Zheng, Y. Jiao, Y. Zhu, L. H. Li, Y. Han, Y. Chen, M. Jaroniec, S. Z. Qiao, *J. Am. Chem. Soc.* **2016**, *138*, 16174-16181.

[19] R. Subbaraman, D. Tripkovic, K. C. Chang, D. Strmcnik, A. P. Paulikas, P. Hirunsit, M. Chan, J. Greeley, V. Stamenkovic, N. M. Markovic, *Nat. Mater.* **2012**, *11*, 550-557.

[20] G. Sheng, J. Chen, Y. Li, H. Ye, Z. Hu, X.-Z. Fu, R. Sun, W. Huang, C.-P. Wong, *ACS Appl. Mater. Interfaces* **2018**, *10*, 22248-22256.

[21] Q. Qin, H. Jang, L. Chen, G. Nam, X. Liu, J. Cho, *Adv. Energy Mater.* **2018**, *8*, 1801478.

[22] D. Yoon, J. Lee, B. Seo, B. Kim, H. Baik, S. H. Joo, K. Lee, *Small* **2017**, *13*, 1700052.

[23] G. Chen, T. Wang, J. Zhang, P. Liu, H. Sun, X. Zhuang, M. Chen, X. Feng, *Adv. Mater.* **2018**, *30*, 1706279.

[24] Q. Yao, B. L. Huang, N. Zhang, M. Z. Sun, Q. Shao, X. Q. Huang, *Angew. Chem.-Int. Edit.* **2019**, *58*, 13983-13988.

[25] W. H. Lai, L. F. Zhang, W. B. Hua, S. Indris, Z. C. Yan, Z. Hu, B. Zhang, Y. Liu, L. Wang, M. Liu, R. Liu, Y. X. Wang, J. Z. Wang, Z. Hu, H. K. Liu, S. L. Chou, S. X. Dou, *Angew. Chem., Int. Ed.* **2019**, *58*, 11868-11873.